Supporting Information

Notari et al. 10.1073/pnas.1408111112

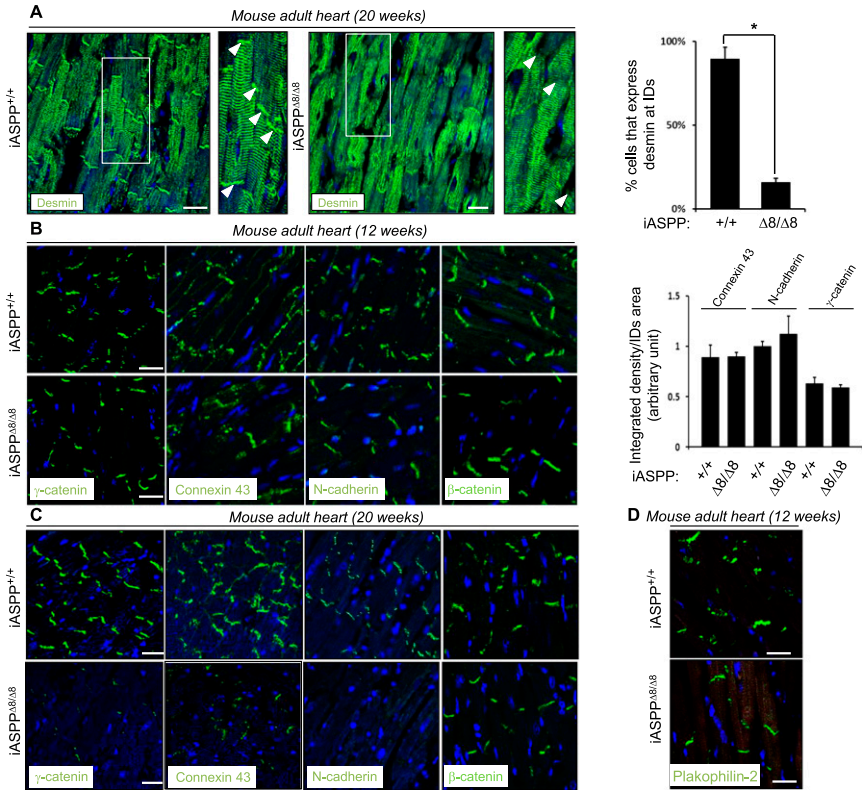

Fig. S1. (*A*, *Left*) Myocardial ventricular cross-sections of 20-wk-old iASPP$^{+/+}$ and iASPP$^{\Delta 8/\Delta 8}$ hearts. Sections were immunostained for desmin. The figure shows classical sarcomeric pattern distribution of the protein in both normal and iASPP mutant hearts. Desmin signal also is concentrated at the intercalated discs region in control tissue but is completely absent in iASPP$^{\Delta 8/\Delta 8}$ hearts (arrowheads). (*Right*) Cells expressing desmin at the intercalated discs were counted (n = 200), and the number obtained was converted to the percentage of cells. (*B* and *C*) Differential expression of intercalated disc components in iASPP$^{+/+}$ and iASPP$^{\Delta 8/\Delta 8}$ mice. Ventricular myocardial sections from 12-wk-old (*B*) or 20-wk-old (*C*) iASPP$^{+/+}$ and iASPP$^{\Delta 8/\Delta 8}$ mice were immunostained using γ-catenin, connexin 43, *N*-cadherin, and β-catenin antibodies. The bar graph in *B* shows the average intensity of the different junctional components. In *C*, note the reduced expression of γ-catenin, connexin 43, and *N*-cadherin, but not β-catenin, in 20-wk-old iASPP mutant hearts compared with the wild type. (*D*) Similar expression of PKP2 was observed on ventricular myocardial sections from 12-wk-old iASPP$^{+/+}$ and iASPP$^{\Delta 8/\Delta 8}$ mice. (Scale bars, 20 μm.)

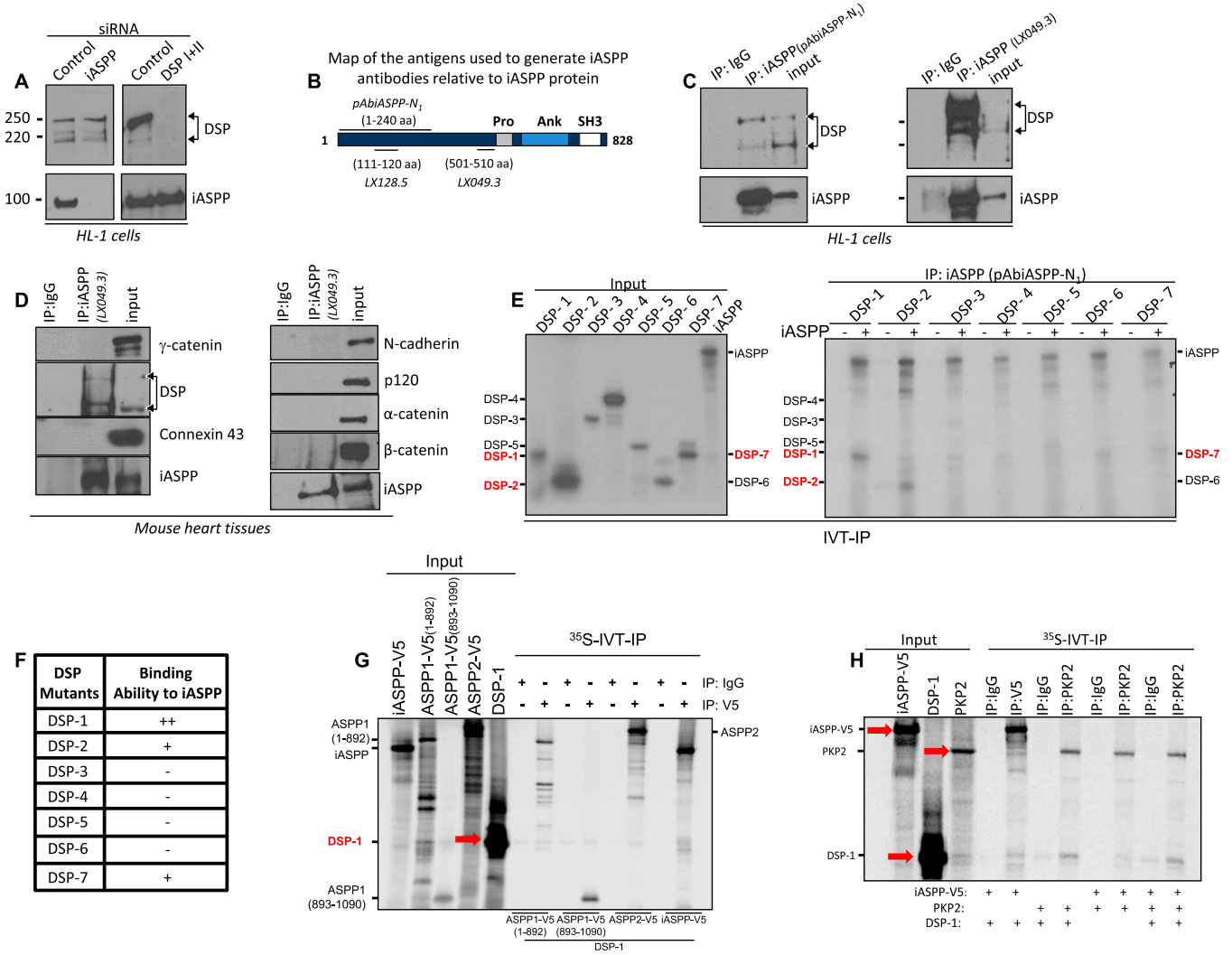

DSP Mutants	Binding Ability to iASPP
DSP-1	++
DSP-2	+
DSP-3	-
DSP-4	-
DSP-5	-
DSP-6	-
DSP-7	+

Fig. S2. (*A*) Western blot analyses of the mouse cardiomyocyte cell line HL-1 transfected with RNAi for iASPP and desmoplakin (DSP) shows that iASPP and the desmoplakin expression level are not interdependent. (*B*) Diagram shows the location of the antigens used to generate the LX128.5-, LX049.3-, and pAbiASPPN$_1$-specific iASPP antibodies relative to full-length iASPP protein. Pro, proline-rich domain; Ank, ankyrin repeats; SH3, Src homology domain. (*C*) The ability of endogenous iASPP protein to interact with endogenous desmoplakin was detected in HL-1 cells using an immunoprecipitation (IP) assay. The mouse anti-iASPP antibody LX049.3 (*Right*) and the rabbit anti-iASPP antibody pAbiASPPN$_1$ (*Left*) were used to immunoprecipitate iASPP. IgG derived from same species was used as a negative control. The presence of desmoplakin was detected with a rabbit or mouse antibody. The membranes were reprobed with an anti-iASPP antibody to determine the amounts of iASPP precipitate. (*D*) The ability of endogenous iASPP protein to interact with endogenous desmoplakin, but not with other junctional components such as γ-catenin, *N*-cadherin, p120, α-catenin, β-catenin, and connexin 43 was detected in adult mouse hearts using an immunoprecipitation assay. The amounts of iASPP precipitate were detected by polyclonal anti-iASPP antibody. (*E*) The ability of iASPP to bind different desmoplakin truncation constructs was measured using in vitro-translated [^{35}S]methionine-labeled iASPP and different desmoplakin truncation mutants. Quantified mean data are shown in Fig. 2*B*. (*F*) The table depicts the different desmoplakin truncated mutants and the ability to bind (+), bind very well (++) or not bind (–) iASPP is presented based on the bar graph in Fig. 2*B*. (*G* and *H*) In vitro-translated [^{35}S]methionine-labeled iASPP-V5, ASPP2-V5, ASPP1-V5 N-terminal (1–892), and ASPP1-V5 C-terminal (893–1090) (*G*) or PKP2 (*H*) and DSP-1(1–394) truncation mutants were used to assess binding between indicated constructs. Red arrows indicate DSP-1 in *G* and iASPP-V5, PKP2, and DSP-1 in *H*.

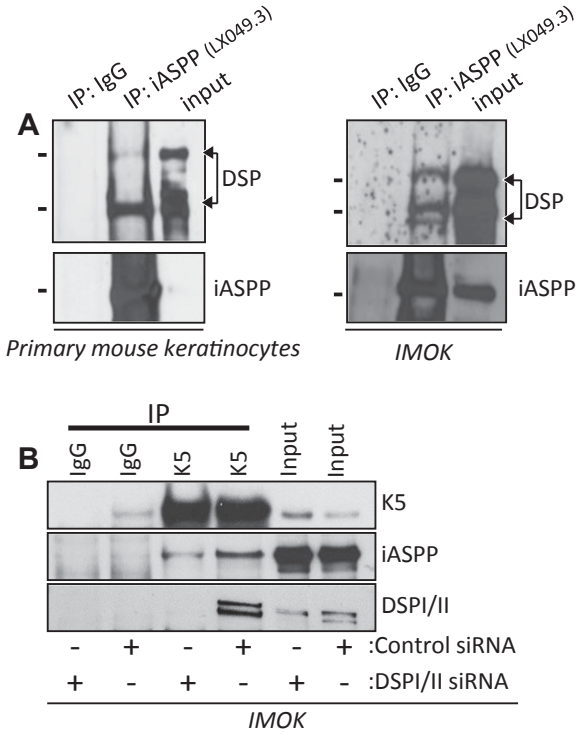

Fig. S3. (*A*) The ability of endogenous iASPP protein to interact with endogenous desmoplakin was detected in primary keratinocytes and IMOK cells using an immunoprecipitation assay. A mouse anti-iASPP antibody, LX049.3, was used to pull down iASPP. IgG derived from mouse was used as a negative control. The presence of desmoplakin was detected with a rabbit antibody. The membranes were reprobed with an anti-iASPP antibody to determine the amounts of iASPP precipitate. (*B*) Keratin 5 was immunoprecipitated from IMOK cells previously treated with scrambled vs. desmoplakin (DSPI/II) siRNA. The coprecipitated keratin 5 and iASPP were detected by blotting with corresponding antibodies as indicated. Immunoblots show that in the presence of desmoplakin siRNA, the binding of immunoprecipitated keratin 5 to iASPP is reduced.

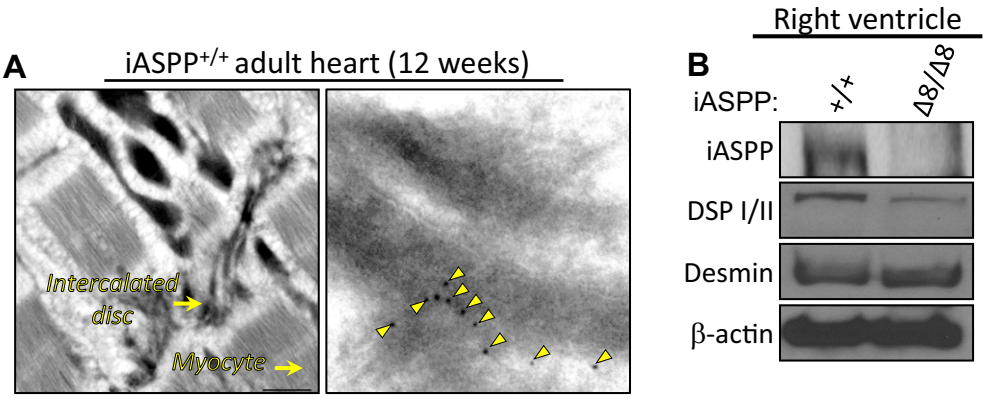

Fig. S4. (*A*) Immunoelectron micrographs of mouse iASPP$^{+/+}$ show a cross-section of the area composita plaque labeled using a specific antibody against iASPP (yellow arrowheads). (*B*) Desmoplakin levels are decreased in the insoluble fraction from the right ventricle of iASPP$^{\Delta 8/\Delta 8}$ animals compared with wild-type controls, but no differences in desmin levels are observed.

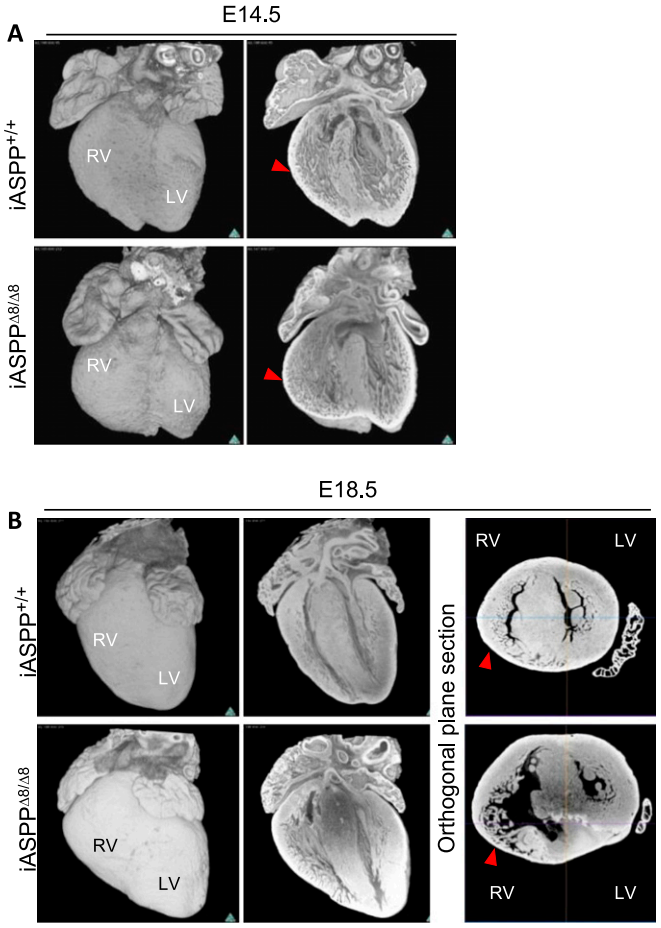

Fig. S5. iASPP-deficient embryos exhibit cardiac right ventricular dilatation. Reconstruction of (*A*) E14.5 and (*B*) E18.5 3D iASPP$^{+/+}$ and iASPP$^{\Delta 8/\Delta 8}$ embryonic hearts from HREM shows progressive heart erosion. (*A*) Right (RV) and left (LV) ventricles are indicated. Note the mild dilation and the thinner right ventricle in E14.5 iASPP$^{\Delta 8/\Delta 8}$ specimens compared with iASPP$^{+/+}$ hearts (red arrowheads). (*B*) The E18.5 iASPP$^{\Delta 8/\Delta 8}$ heart has an obviously distorted morphology in which loss of myocardial tissue is shown by a "blotchy" pattern. The orthogonal plane shows the dilation of the right ventricle and reduced thickness of the right ventricular wall (red arrowhead).

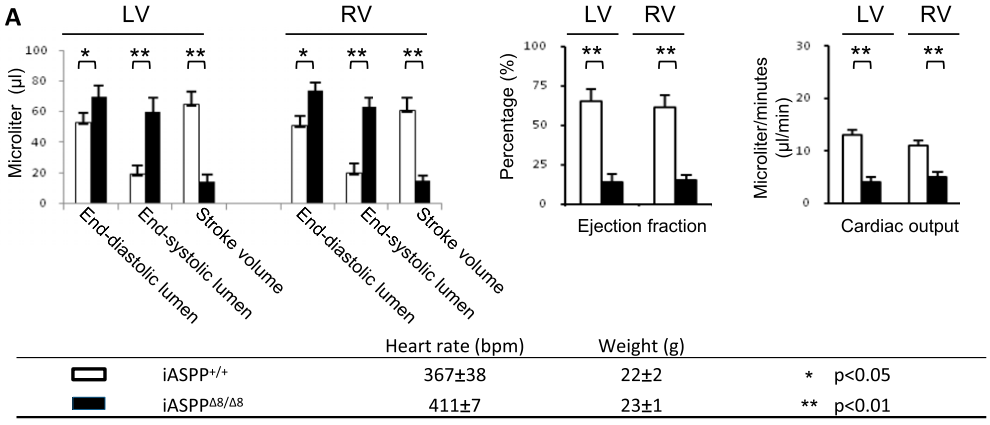

		Heart rate (bpm)	Weight (g)		
▭	iASPP$^{+/+}$	367±38	22±2	*	p<0.05
■	iASPP$^{\Delta 8/\Delta 8}$	411±7	23±1	**	p<0.01

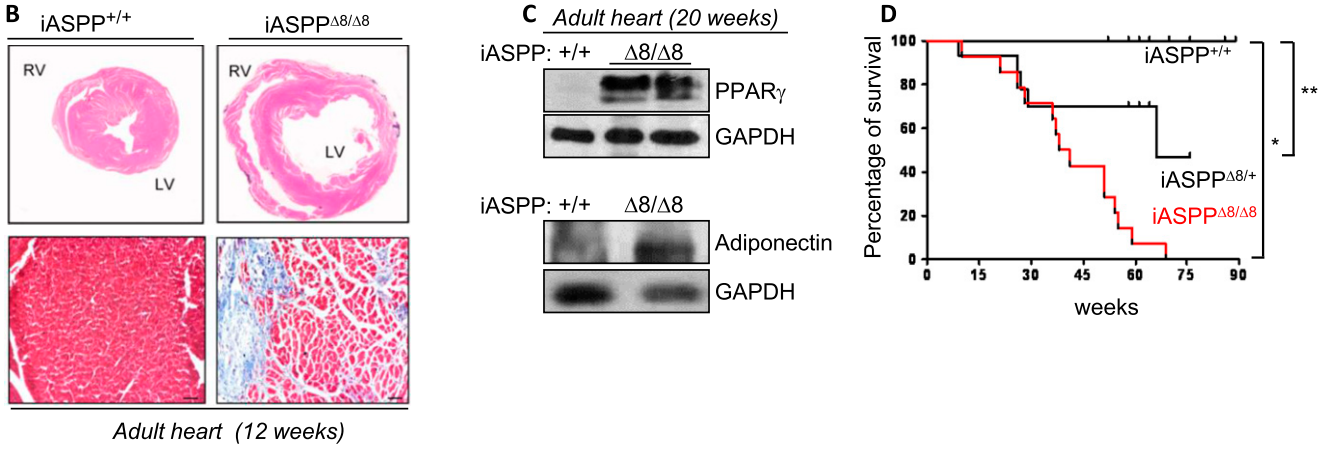

Fig. S6. (*A*) Twelve-week-old adult iASPP-null mice show impaired cardiac function as assessed by left ventricle and right ventricle end-diastolic lumen, end-systolic lumen, stroke volume, ejection fraction, and cardiac output. Bar graphs illustrate structural and functional parameters obtained from MRI screening of iASPP$^{+/+}$ and iASPP$^{\Delta 8/\Delta 8}$ mice. *$P < 0.05$, **$P < 0.01$ compared with iASPP$^{+/+}$ mice. Heart rate and body weight are similar in the two groups. (*B*) Cross-sections from iASPP$^{+/+}$ and iASPP$^{\Delta 8/\Delta 8}$ hearts were stained using H&E (*Upper*) and Masson's trichrome (*Lower*). Note the dilated ventricles in the iASPP$^{\Delta 8/\Delta 8}$ heart (*Upper*), myocardial disarray associated with increased intercellular spaces between cardiomyocytes, and fibrotic deposits (*Lower*). (Scale bars, 50 μm.) (*C*) Expression of PPARγ and adiponectin were analyzed by Western blot analyses in wild-type and iASPP-deficient hearts. GAPDH was used as a loading control. (*D*) Kaplan–Meier survival curve of iASPP$^{+/+}$ ($n = 20$), iASPP$^{\Delta 8/+}$ ($n = 20$), and iASPP$^{\Delta 8/\Delta 8}$ ($n = 22$) mice. Sex did not affect the mortality rate of iASPP$^{\Delta 8/\Delta 8}$ mice. By 40 wk of age, only 50% of iASPP$^{\Delta 8/\Delta 8}$ mice survived. Gross analyses of the iASPP$^{\Delta 8/\Delta 8}$ hearts revealed that all the iASPP mutant mice had developed dilated cardiomyopathy ($n = 22$).

A

clinical diagnosis	*iASPP*	*N-cadh*	*γ-cat*
normal	↔	↔	↔
ARVC	↓↓	↔	↔
ARVC	↓	*N.A.*	*N.A.*
normal	↔	↔	*N.A.*
ARVC	↓	↔	↔
normal	↔	↔	*N.A.*
ARVC	↓	*N.A.*	*N.A.*
ARVC	↓	↔	*N.A.*
ARVC	↔	↔	*N.A.*
ARVC	↔	↔	*N.A.*

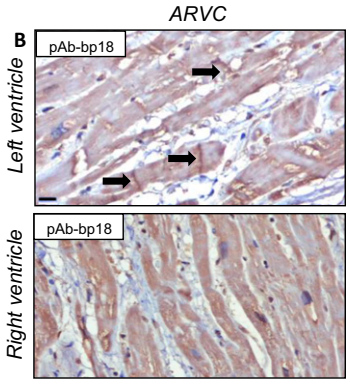

Fig. S7. Immunohistochemistry of ventricular myocardium from unaffected and ARVC-affected subjects. (*A*) Clinical and immunohistochemical summary of human cardiac sections analyzed. ↔, basal level; ↓, reduced level; N.A., not available. (*B*) Immunohistochemistry of iASPP shows a differential expression at cell–cell junctions in the left (black arrow) and right myocardial sections in one of the ARVC samples analyzed. (Scale bars, 20 μm.)